

# Ca<sup>2+</sup> Hot Spots on the Mitochondrial Surface Are Generated by Ca<sup>2+</sup> Mobilization from Stores, but Not by Activation of Store-Operated Ca<sup>2+</sup> Channels

Marta Giacomello,<sup>1,5</sup> Ilaria Drago,<sup>1,5</sup> Mario Bortolozzi,<sup>2</sup> Michele Scorzeto,<sup>3</sup> Alessio Gianelle,<sup>4</sup> Paola Pizzo,<sup>1</sup> and Tullio Pozzan<sup>1,2,\*</sup>

<sup>1</sup>Department of Biomedical Sciences, University of Padova and CNR Neuroscience Institute, Via G. Colombo 3, 35121 Padova, Italy

<sup>2</sup>Venetian Institute of Molecular Medicine, Viale Giuseppe Orus 2, 35131 Padova, Italy

<sup>3</sup>Department of Human Anatomy and Physiology, University of Padova, Via Francesco Marzolo 3, Padova 35131, Italy

<sup>4</sup>Istituto Nazionale di Fisica Nucleare, Via Enrico Fermi 41, 00044 Frascati, Italy

<sup>5</sup>These authors contributed equally to this work

\*Correspondence: tullio.pozzan@unipd.it

DOI 10.1016/j.molcel.2010.04.003

## SUMMARY

Although it is widely accepted that mitochondria in living cells can efficiently uptake Ca<sup>2+</sup> during stimulation because of their vicinity to microdomains of high [Ca<sup>2+</sup>], the direct proof of Ca<sup>2+</sup> hot spots' existence is still lacking. Thanks to a GFP-based Ca<sup>2+</sup> probe localized on the cytosolic surface of the outer mitochondrial membrane, we demonstrate that, upon Ca<sup>2+</sup> mobilization, the [Ca<sup>2+</sup>] in small regions of the mitochondrial surface reaches levels 5- to 10-fold higher than in the bulk cytosol. We also show that the [Ca<sup>2+</sup>] to which mitochondria are exposed during capacitative Ca<sup>2+</sup> influx is similar between near plasma membrane mitochondria and organelles deeply located in the cytoplasm, whereas it is 2- to 3-fold higher in subplasma membrane mitochondria upon activation of voltage-gated Ca<sup>2+</sup> channels. These results demonstrate that mitochondria are exposed to Ca<sup>2+</sup> hot spots close to the ER but are excluded from the regions where capacitative Ca<sup>2+</sup> influx occurs.

## INTRODUCTION

Mitochondrial Ca<sup>2+</sup> transport plays a key role in the regulation of a variety of physiological functions and in modulating cell death (Orrenius et al., 2003; Rizzuto et al., 2003, 2004; Rizzuto and Pozzan, 2006). Direct measurement of matrix Ca<sup>2+</sup> concentration, [Ca<sup>2+</sup>]<sub>m</sub>, revealed that, at rest, [Ca<sup>2+</sup>]<sub>m</sub> is indistinguishable from the cytosolic Ca<sup>2+</sup> concentration, [Ca<sup>2+</sup>]<sub>c</sub>; in response to stimulation, however, [Ca<sup>2+</sup>]<sub>m</sub> can reach values up to 10- to 100-fold higher than in the cytoplasm (Rizzuto et al., 2004). The high speed of mitochondrial Ca<sup>2+</sup> uptake in living cells in response to relatively small increases in [Ca<sup>2+</sup>]<sub>c</sub> contrasts with the known low affinity of the mitochondrial Ca<sup>2+</sup> uniporter (K<sub>d</sub> about 20–50 μM) as measured in vitro or in permeabilized cells

under conditions mimicking those of the cytosol. This paradox was explained by the so-called “Ca<sup>2+</sup> microdomain hypothesis” whereby the efficiency of mitochondria at accumulating Ca<sup>2+</sup> in living cells depends on the strategic localization of the organelles close to Ca<sup>2+</sup> channels, regions where [Ca<sup>2+</sup>] can transiently reach levels higher than in the bulk cytosol, such as, for example, in the proximity of IP<sub>3</sub>- or ryanodine-sensitive endoplasmic/sarcoplasmic reticulum (ER/SR) channels (Rizzuto et al., 1998).

The “Ca<sup>2+</sup> microdomain hypothesis” is supported by a number of studies from different laboratories (see, among others, Collins et al., 2001; Montero et al., 2000; Pacher et al., 2002; Rizzuto et al., 1993), but direct experimental proof for their existence, localization, and the quantitative measurement of the size, duration, and [Ca<sup>2+</sup>] of these hot spots is still lacking. In addition, a number of indirect results challenging the microdomain hypothesis have been largely neglected. For example, major ER or mitochondria remodelling has no major effect on Ca<sup>2+</sup> accumulation by the latter organelle (Rutter, 2006), whereas in some cell types, Ca<sup>2+</sup> uptake by mitochondria is small and slow, despite substantial increases in [Ca<sup>2+</sup>]<sub>c</sub> (Babcock et al., 1997; Lawrie et al., 1996). The only studies, to our knowledge, that have directly addressed in quantitative terms the existence of Ca<sup>2+</sup> hot spots close to mitochondria have been those of Rizzuto et al. (1998) and Brandenburger et al. (1999), using aequorin constructs localized in the intermembrane space or on the cytosolic surface of the outer mitochondrial membrane, OMM, respectively. In the first study, it was demonstrated that the mean [Ca<sup>2+</sup>] sensed by this probe in response to Ca<sup>2+</sup> release from IP<sub>3</sub>-sensitive ER channels is slightly higher than average [Ca<sup>2+</sup>]<sub>c</sub>, whereas in the second, no significant difference was observed. The discrepancy may depend on the fact that aequorin could only monitor the average of the cell population and not the single cell (and organelle) behavior, and thus local differences in a subpopulation of organelles may be overlooked.

In the present study, we developed probes derived from a family of GFP-based Ca<sup>2+</sup> indicators (Palmer et al., 2006) that are capable of monitoring [Ca<sup>2+</sup>] selectively at the cytosolic surface of the OMM and in the nucleoplasm. We directly demonstrate that, indeed, high Ca<sup>2+</sup> microdomains can be generated close to some mitochondria upon opening of IP<sub>3</sub>-gated Ca<sup>2+</sup>

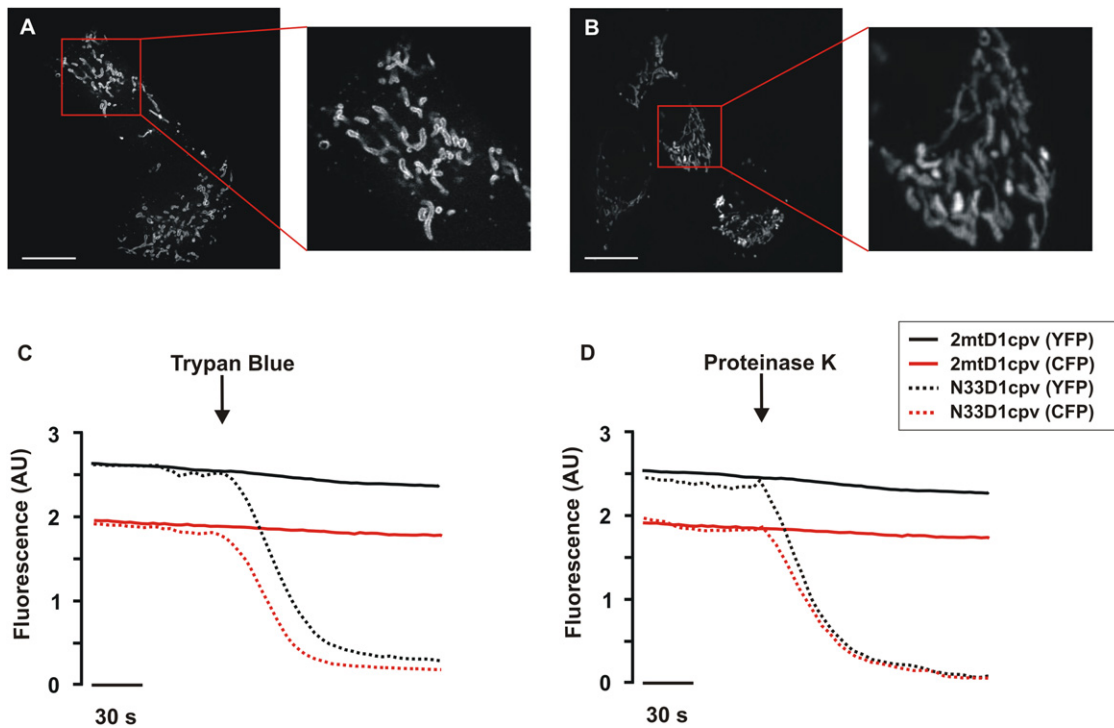


**Figure 1. Characterization of N33D1cpv Localization**

(A and B) Typical fluorescence pattern obtained by video confocal imaging of HeLa cells expressing N33D1cpv (A) or a 2mtD1cpv (B). On the right, a section of the images was enlarged to better appreciate the different staining pattern of N33D1cpv and 2mtD1cpv. Scale bar, 10  $\mu$ m.

(C and D) HeLa cells expressing either N33D1cpv (dotted trace) or 2mtD1cpv (continuous trace) were permeabilized with digitonin in an intracellular-like medium without added CaCl<sub>2</sub> and supplemented with 1 mM EGTA and treated with trypan blue (C) or proteinase K (D). The black and red traces represent the fluorescence of YFP and CFP (arbitrary units [AU]), respectively. The fluorophores were excited at 425 nm or 480 nm, and the emissions were collected at 480 or 540 nm for CFP and YFP, respectively.

channels of the ER. We also show that, whereas activation of voltage-operated Ca<sup>2+</sup> channels (VOCCs) results in substantially larger rises of [Ca<sup>2+</sup>]<sub>i</sub> at the OMM of organelles close to the plasma membrane than in more deeply located mitochondria, upon activation of capacitative Ca<sup>2+</sup> entry (CCE), no difference between the two organelle populations is observed, suggesting that mitochondria are excluded from the regions where store-operated Ca<sup>2+</sup> channels are activated.

## RESULTS

### Generation of New, GFP-Based Ca<sup>2+</sup> Indicators Selectively Localized at the Cytosolic Surface of the OMM

Palmer et al. (2006) have recently described a family of GFP-based Ca<sup>2+</sup> indicators, the Dcpv family, derived from cameleons. These probes have been engineered to drastically reduce the competition by endogenous calmodulin, and a number of variants have been generated, with different Ca<sup>2+</sup> affinities. We focused on D1cpv, whose K<sub>d</sub> for Ca<sup>2+</sup> in vitro spans a large concentration range and is suitable to monitor Ca<sup>2+</sup> changes from less than 1  $\mu$ M up to 200–300  $\mu$ M.

A chimera of TOM20 (a component of the mitochondrial protein import machinery, endogenous of the OMM) with GFP has been specifically targeted to mitochondria when expressed

in HeLa cells (Kanaji et al., 2000 and our unpublished data). The fusion protein TOM20-D1cpv, when transiently expressed, showed a diffuse staining (data not shown), indistinguishable from that of cytosolic D1cpv. However, when only the first 33 amino acids of the TOM20 N-terminal tail (N33; known to contain the mitochondrial anchoring signal; Kanaji et al., 2000) were fused to D1cpv, the expressed chimeric protein exhibited a staining pattern that closely resembled that of D1cpv located in the mitochondrial matrix (2mtD1cpv) (Figures 1A and 1B).

Though both probes were localized in a complex convoluted tubular network and on small round organelles, the fine staining pattern (better appreciated in the enlarged panels of Figure 1) was significantly different. In the cell expressing N33D1cpv (Figure 1A), the labeling is distributed on the surface of the tubules (most likely the OMM), with a clear low-fluorescence region in between (most likely the matrix). In the case of the matrix-located probe (Figure 1B), on the contrary, the mitochondria appeared homogeneously fluorescent. A staining pattern similar to that of N33D1cpv was observed when untransfected cells were stained with an anti-TOM20 antibody (data not shown). The localization of N33D1cpv on the OMM was further verified by the experiments presented in Figures 1C and 1D. In Figure 1C, cells expressing N33D1cpv or 2mtD1cpv were first treated with digitonin (that selectively permeabilizes the plasma membrane, leaving largely intact internal membranes) and then

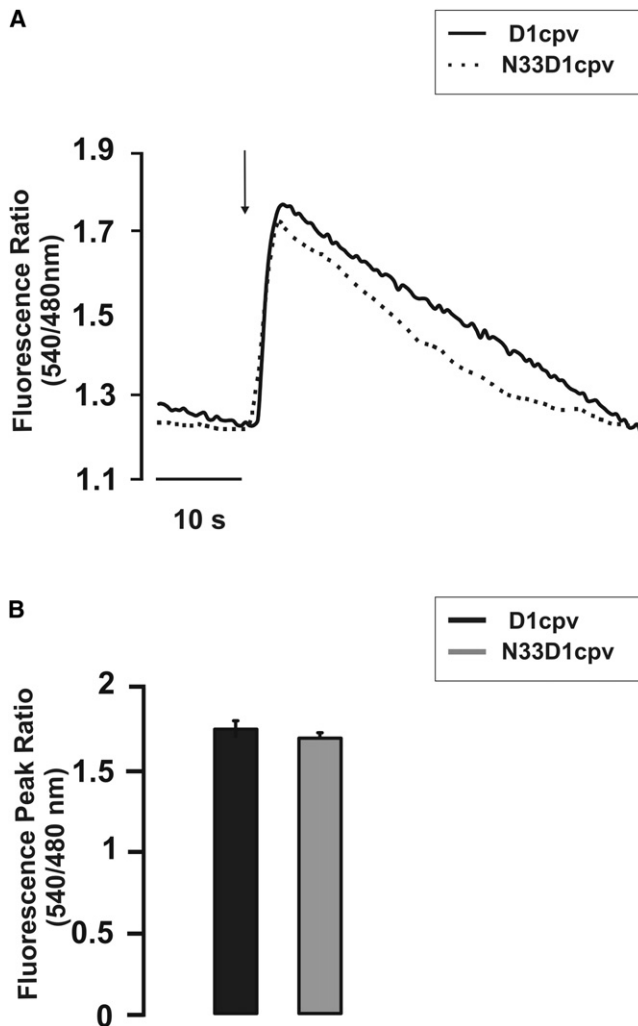


**Figure 2. [Ca<sup>2+</sup>]<sub>i</sub> Increases Induced by Histamine as Measured in the Cytosol and on the OMM**

(A) Kinetics of the fluorescence changes of typical HeLa cells expressing N33D1cpv (dotted trace) or cytosolic D1cpv (continuous trace). Cells were bathed in extracellular medium; no CaCl<sub>2</sub> was added, and EGTA (100 μM) was added 1 min before stimulation with histamine (200 μM; arrow). (B) Mean increases of the [Ca<sup>2+</sup>]<sub>i</sub> in the cytoplasm and OMM elicited by histamine (Student's *t* test, not significant). The data are expressed as the peak ratio of the fluorescence emitted at 540/480 nm ± SEM.

with the dye trypan blue, a strong fluorescence quencher (Sahlin et al., 1995). Upon addition of the dye to N33D1cpv-expressing cells, both CFP and YFP signals were rapidly quenched (Figure 1C, dotted traces); on the contrary, no fluorescence quenching was observed in cells expressing 2mtD1cpv (Figure 1C, continuous traces). In the experiment presented in Figure 1D, cells expressing either N33D1cpv or 2mtD1cpv were permeabilized with digitonin and then treated with proteinase K; the fluorescence signal of N33D1cpv (dotted traces) was rapidly abolished by the protease, while that of 2mtD1cpv (continuous traces) was not affected. Further evidence confirms that N33D1cpv is indeed localized on the OMM (and facing the cytosol): (1) proteinase K had no effect on the fluorescence of

cells expressing cytochrome C-GFP (Figure S1 available online) and (2) in N33D1cpv-expressing cells permeabilized with digitonin and then incubated with a polyclonal anti-GFP antibody (that recognizes both CFP and YFP), a typical mitochondrial staining was observed (Figure S2A). In parallel, untransfected cells were treated in the same way but with an anti-cytochrome C antibody; no staining was observed in this latter case (Figure S2B). In cells permeabilized with methanol, according to the standard protocol, and treated with the anti-cytochrome C antibody, the typical mitochondrial staining was observed (Figure S2C).

Finally, when HeLa cells, expressing either N33D1cpv or 2mtD1cpv, were challenged with an IP<sub>3</sub>-generating stimulus, histamine, in the presence of a mitochondrial uncoupler, the Ca<sup>2+</sup> signal was suppressed in cells expressing 2mtD1cpv and was hardly affected in the other case (data not shown).

### Ca<sup>2+</sup> Measurements

Figure 2A shows the typical average response to the Ca<sup>2+</sup>-mobilizing stimulus histamine of two cells expressing either N33D1cpv or D1cpv. The average peak of the 540/480 fluorescence emission ratio in cells expressing D1cpv targeted either to the OMM or cytosol were similar (Figure 2B). These results could be interpreted as evidence against the existence of Ca<sup>2+</sup> microdomains around mitochondria or as an indication that microdomains are obscured by the signal of the majority of the probe exposed to bulk [Ca<sup>2+</sup>]<sub>c</sub>.

To address the issue in greater detail, we performed a “pixel-by-pixel” analysis of the ratio images; small mitochondrial regions (~20% of the cell volume) were randomly selected for ratio analyses. In Figure 3B, the images of one such region, before and during the first 1.5 s after the histamine challenge, are presented. Pixels that exceeded the maximum mean rise in ratio (induced by histamine) by 20% were color coded red in the figures. In the case of both cytosolic- (data not shown) and OMM-targeted D1cpv, scattered red pixels appeared during the [Ca<sup>2+</sup>]<sub>c</sub> rise induced by histamine. Red pixels were most often clustered in groups of two to four adjacent pixels (see below). The kinetics (one image every 300 ms) of the mean increase in 540/480 fluorescence emission ratio (expressed as ΔR increase) from five regions (of five different cells) is presented in Figure 3A. The peak value was reached, on average, in 0.9 s (range 0.6–2 s). In Figure 3C, the percentage of red pixels (from a large number of cells in different experiments) was plotted as a function of the mean ratio value of the region (i.e., from basal, up to the peak of histamine). The percentage of red pixels was clearly higher for the N33D1cpv than for the cytosolic D1cpv for small increases in mean ratio (i.e., during the upstroke of the [Ca<sup>2+</sup>]<sub>c</sub> rise) and then became almost indistinguishable for the two probes.

The percentage of red pixels in the cytosol or OMM of cells treated with cyclopiazonic acid (CPA) was then monitored. CPA is an inhibitor of the ER Ca<sup>2+</sup> pump and causes a passive release of Ca<sup>2+</sup> from the organelle without generating Ca<sup>2+</sup> hot spots (Collins et al., 2001). In Figure 3D, it is shown that not only the percentage of red pixels measured in response to CPA in the cytosol or OMM are indistinguishable, but also that, for the same average rise in [Ca<sup>2+</sup>]<sub>c</sub>, they are much less frequent than when histamine was used as stimulus.

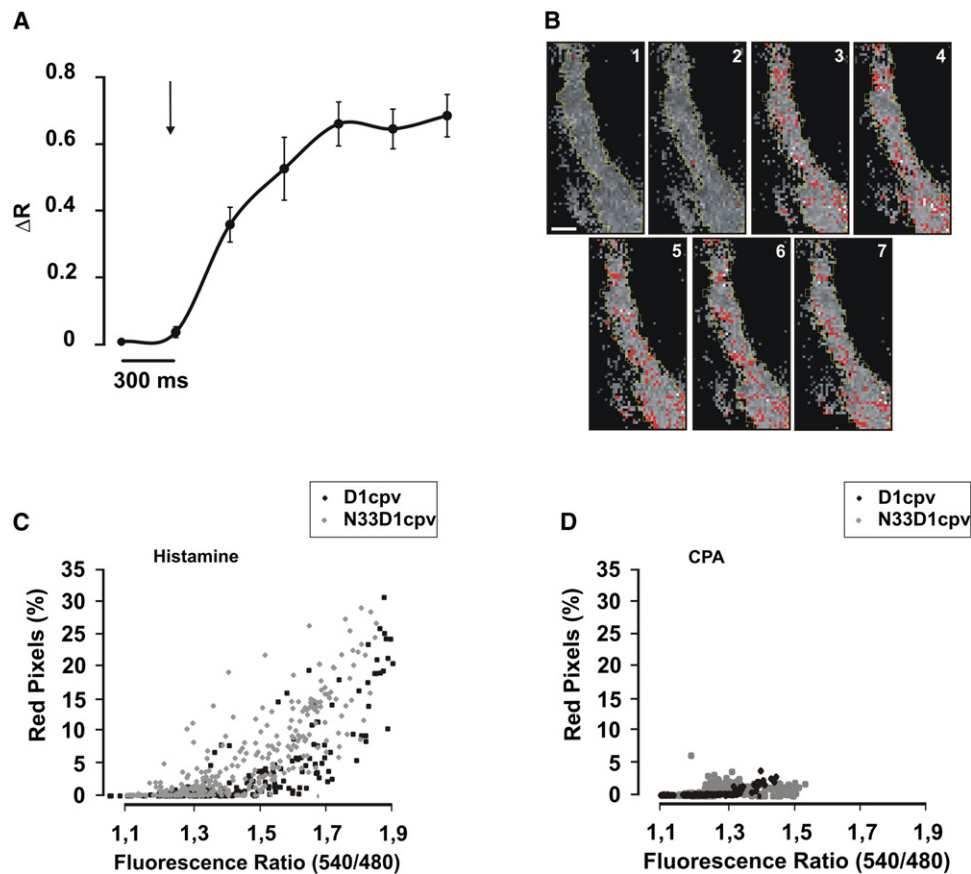


**Figure 3. Pixel-by-Pixel Analysis of the [Ca<sup>2+</sup>] Changes Elicited by Histamine on the OMM**

(A) Typical kinetic of the 540/480 fluorescence emission ratio changes, averaged over mitochondrial regions, upon histamine stimulation of HeLa cells transiently transfected with N33D1cpv (mean of five cells  $\pm$  SD). Histamine (200  $\mu$ M) was added where indicated by the arrow. The 540/480 fluorescence emission ratio is here expressed as  $\Delta R$  over the basal value.

(B) Sequence of the individual 540/480 nm ratio values of a region in a typical cell (one image every 300 ms). The maximum average 540/480 nm peak fluorescence emission ratio of this region caused by histamine was 1.72, and every pixel with an intensity ratio between 2 and 2.5 was color coded red. Pixels with ratio values above 2.5 were color coded white. Scale bar, 1  $\mu$ m.

(C and D) Cells transfected with N33D1cpv (gray symbol) or D1cpv (black symbol). Each point represents the percentage of red pixels of one image (analyzed as in B) plotted as a function of the mean ratio value of the whole region, from basal conditions up to the peak caused by either histamine (200  $\mu$ M; C) or CPA (50  $\mu$ M; D). Other conditions were as in Figure 2. When the [Ca<sup>2+</sup>]<sub>i</sub> returned to basal levels, the percentage of red pixel returned to the level before histamine addition.

A simple analysis as that presented in Figure 3 is subjected to potential artifacts due to random noise of the camera and numerical computation of the ratio images. A more stringent analysis was thus developed (for details, see [Supplemental Experimental Procedures](#)). In order to reduce statistical noise, the single pixels were spatially and temporally smoothed. In addition, due to the variability among experiments of the absolute values of the 540/480 nm ratio at rest and at the peak of a histamine challenge, in all of the following experiments, the data have been calculated as  $\Delta R/R_0$  (in which  $\Delta R$  is the change in 540/480 nm emission ratio, and  $R_0$  is the value of the 540/480 nm emission ratio before addition of histamine). Figure 4A shows the typical time course of  $\Delta R/R_0$ , spatially averaged over the whole cell expressing N33D1cpv. Figure 4B shows the histogram (with superimposed [red trace] Gaussian fit, see below) of the maximum  $\Delta R/R_0$  value ( $\Delta R_{\max}/R_0$ ) reached by each single pixel in the cell analyzed in 4A (cumulative of the first 4 s of the histamine challenge). Figure 4C

and 4D show, respectively, the 2D and 3D images of  $\Delta R_{\max}/R_0$  on the OMM of the same cell. A threshold was established so that pixels with  $\Delta R_{\max}/R_0$  higher than 125% of the mean value (taken as 100%) were yellow-to-red color coded and superimposed to the mitochondrial YFP fluorescence (black and white). Unlike the analysis of Figure 3, the colored pixels do not refer to a single image but, rather, to all of the pixels that exceeded the mean  $\Delta R_{\max}/R_0$  value in the first 4 s following the addition of histamine. Of note, using this more stringent analysis, the clustering of hot spots is more obvious than the crude unprocessed images of Figure 3, though the number of hot pixels is lower (suggesting that, in the former analysis, hot pixels were, in part, due to noise or to very small hot spots that are lost upon smoothing). The percentage of pixels exceeding 125% of the mean peak (again normalized as 100%) during the first 4 s of a histamine-induced [Ca<sup>2+</sup>]<sub>i</sub> transient was 11.4% in this cell and  $9.5\% \pm 2.5\%$  (mean  $\pm$  SD) in five cells, expressing N33D1cpv, analyzed

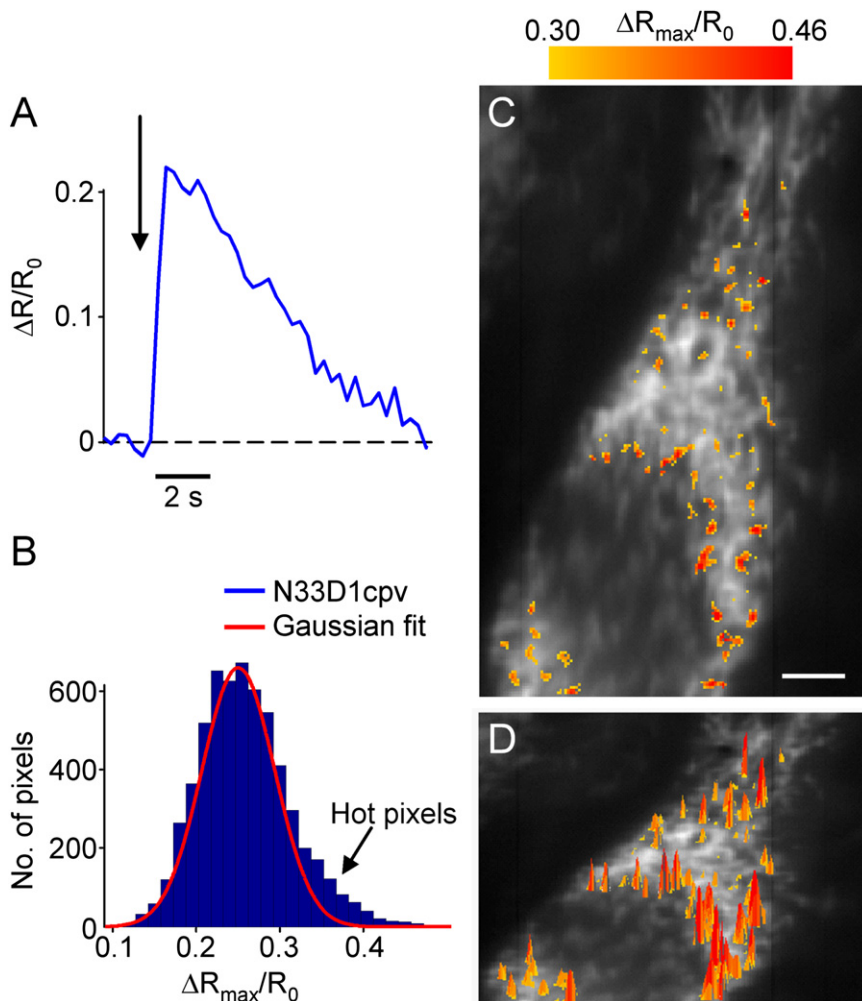


**Figure 4. Pixel-by-Pixel Correlation Analysis of the [Ca<sup>2+</sup>] Changes on the OMM**

(A) Time course of the spatially averaged  $\Delta R/R_0$  signal in a cell transfected with N33D1cpv. Arrow indicates histamine (200  $\mu\text{M}$ ) application.

(B) The maximum  $\Delta R/R_0$  value ( $\Delta R_{\text{max}}/R_0$ ) reached by each single pixel during the first 4 s after histamine stimulus was stored in a histogram of numerosness (bin equals 0.05), which shows the  $\Delta R_{\text{max}}/R_0$  value distribution of 5800 fluorescent pixels. The Gaussian fit (red trace) of the distribution is superimposed to highlight the right tail due to hot pixels.

(C) Yellow-to-red color representation of  $\Delta R_{\text{max}}/R_0$  spatial distribution of pixels in (B) over the threshold of 0.30, equivalent to 125% of the  $\Delta R_{\text{max}}/R_0$  mean. The color pixels are superimposed to mitochondria YFP fluorescence image. (D) Same as (C) with a third dimension to better visualize the distribution of the  $\Delta R_{\text{max}}/R_0$  peaks. Scale bar, 5  $\mu\text{m}$ . Pixel size:  $0.2 \times 0.2 \mu\text{m}$ . Other conditions were as in Figure 3.

in the Ca<sup>2+</sup> peaks of large nuclear or cytosolic regions was practically indistinguishable in cells expressing either D1cpv or H2BD1cpv (the nuclear rise was  $102\% \pm 2.9\%$  of that in the cytosol). In addition, in the few cells expressing D1cpv in which the probe was not excluded from the nucleus, the Ca<sup>2+</sup> peaks, measured within the same cell in the cytosol and in the nucleus, were again very similar (taken as 100% the value of  $\Delta R/R_0$  in the cytosol, that of the nucleus was  $102\% \pm 0.48\%$ ). Finally, in cells cotransfected with the nuclear-

and OMM-located D1cpv, the mean changes in  $\Delta R/R_0$  are similar, though not identical (taken as 100% the values of the nucleus, that of the OMM was  $96.5\% \pm 2.35\%$ ).

We thus applied the same approach used in Figure 4 to cells cotransfected with OMM- and nucleus-targeted D1cpv and stimulated with histamine in Ca<sup>2+</sup>-free medium. Figure 5A shows that, in a typical cell, though the mean  $\Delta R/R_0$  are very similar in amplitude and kinetics in the two compartments, the hot spots during a histamine challenge were abundant and scattered on the OMM and practically absent in the nucleus (Figures 5C and 5D). In Figure 5D, a cell cotransfected with nuclear and cytosolic D1cpv was analyzed by the same approach. The average peak values appear very similar in the two compartments, and the percentage of hot spots is very low in both cases (Figure 5E). In five cells cotransfected with N33D1cpv and H2BD1cpv or cytosolic D1cpv and the nuclear probe, the percentages of hot spots 125% above the mean peaks value were  $9.2\% \pm 2.1\%$  in the case of mitochondria and around 1% for the nucleus and the cytosol.

Concerning the pixel distribution in each image, one would predict that the existence of hot spots on the OMM next to release sites would result in either an extended tail or the

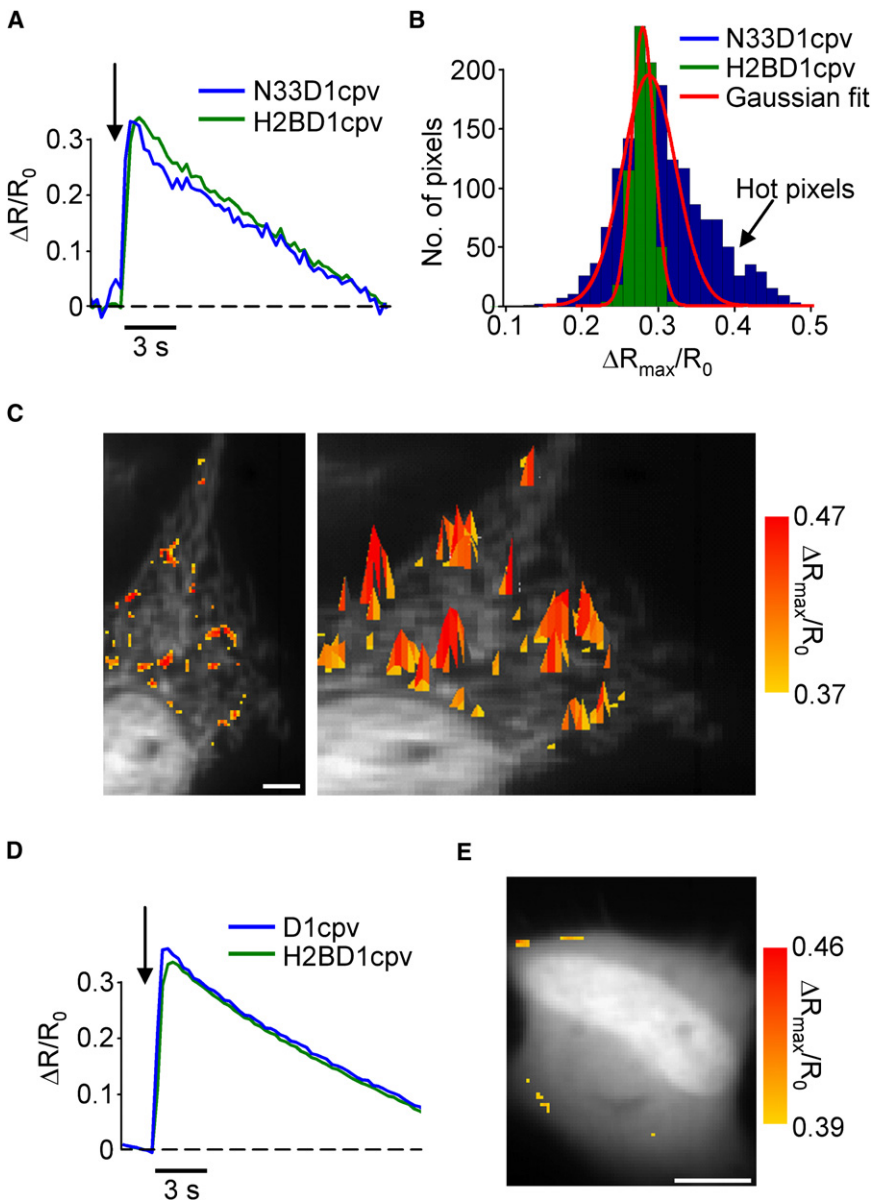


**Figure 5. Comparison of Hot Spot Distribution on the OMM, Nucleoplasm, and Cytoplasm in Cotransfected Cells**

(A) Time course of  $\Delta R/R_0$  spatially averaged over the whole nucleoplasm or mitochondria in a typical cell cotransfected with H2BD1cpv and N33D1cpv.

(B) The nuclear pixel distribution of (A) (green) is much tighter than the mitochondrial one (blue). Moreover, whereas the nuclear  $\Delta R_{\max}/R_0$  distribution almost perfectly fits a Gaussian distribution (red traces), that of mitochondria shows an abnormal right tail.

(C) Two-dimensional (left) and three-dimensional (right) representation of hot pixels as defined in Figure 4.

(D and E) As (A) and (C), but for a cell cotransfected with H2BD1cpv and D1cpv.

Scale bars, 5  $\mu\text{m}$ . All other conditions as in Figure 4.

presence of a second peak. On the contrary, the pixel distribution in the nucleus should be fitted by a normal Gaussian distribution. Indeed, the distribution of the pixel ratio intensities in the case of the nucleus almost perfectly fits a Gaussian distribution (Figure 5B); on the contrary, that on the OMM (Figures 4B and 5B) shows a clear abnormal right tail. Such an abnormal tail has been observed in all of the experiments analyzed.

#### Calibration of the New Probes

The question then arises regarding the absolute  $[\text{Ca}^{2+}]$  reached in the cytosol and on the OMM. In order to calculate the absolute values of the  $[\text{Ca}^{2+}]$  in the various compartments, the in situ  $K_d$  for  $\text{Ca}^{2+}$  of the two probes should be determined. To this end, we used the passive calibration method in digitonin-permeabilized cells previously described (Rudolf et al., 2006; Drago et al.,

2008). D1cpv, however, is rapidly lost upon plasma membrane permeabilization. We thus compared the  $K_d$  for  $\text{Ca}^{2+}$  of N33D1cpv and H2BD1cpv, based on the assumption that cytosolic and nuclear  $[\text{Ca}^{2+}]$  are indistinguishable. After digitonin permeabilization, HeLa cells expressing the two probes were perfused with an intracellular-like medium and variable concentration of  $\text{Ca}^{2+}$  (see Supplemental Experimental Procedures). As observed by Palmer et al. (2006), the calibration curve is not a simple Michaelis-Menten plot but, rather, shows one flex with an apparent steady state at around 10  $\mu\text{M}$   $[\text{Ca}^{2+}]$ .

According to the calibration of Figure S4 (and see Supplemental Experimental Procedures), the average  $[\text{Ca}^{2+}]$  peaks in response to histamine in cells coexpressing the nucleus- and OMM-targeted D1cpv were significantly higher

for the OMM ( $1.58 \pm 0.13 \mu\text{M}$  and  $2.94 \pm 0.25 \mu\text{M}$  for the nucleus and OMM, respectively). The hot spots during a histamine-induced peak can reach  $[\text{Ca}^{2+}]$  between 3.78 and 16.42  $\mu\text{M}$  over the OMM and between 1.9 and 5.47  $\mu\text{M}$  in the nucleus.

#### Near Plasma Membrane Ca<sup>2+</sup> Hot Spots

Histamine is an IP<sub>3</sub>-generating stimulus, and most of the  $[\text{Ca}^{2+}]_i$  rise elicited by this agonist depends on the release of  $\text{Ca}^{2+}$  from the ER.  $\text{Ca}^{2+}$  hot spots are thus expected to occur close to these channels. It should be noted, however, that  $\text{Ca}^{2+}$  hot spots may be generated also around mitochondria close to the plasma membrane when  $\text{Ca}^{2+}$  influx is activated. When we applied the procedure described in Figure 4 to the peak elicited by re-addition of  $\text{Ca}^{2+}$  to cells stimulated with histamine in  $\text{Ca}^{2+}$ -free medium, the percentage of hot spots was negligible (data not

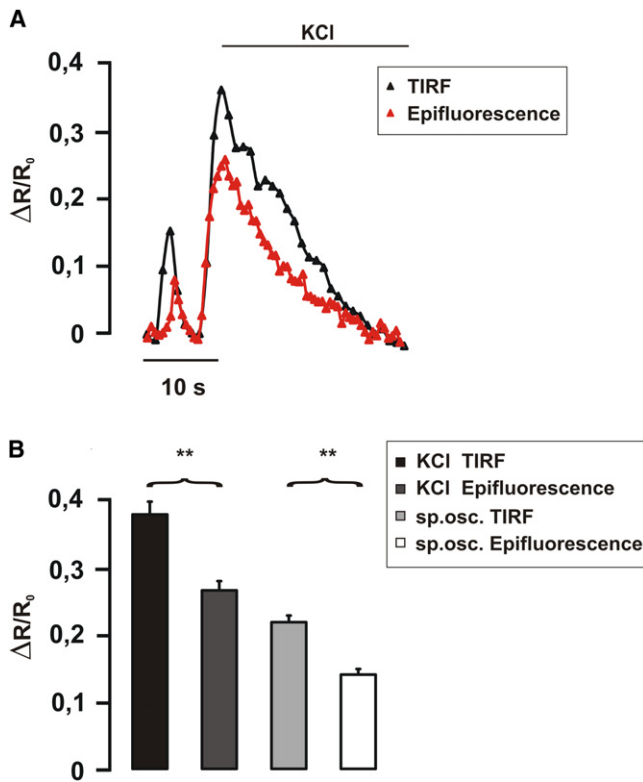


**Figure 6. [Ca<sup>2+</sup>] Changes in the OMM as Measured by TIRF and Epifluorescence in GH3 cells**

(A) Typical kinetics of  $\Delta R/R_0$  in two GH3 cells transiently transfected with N33D1cpv, as measured with TIRF (black trace) or epifluorescence (red trace). The first peak occurs spontaneously, and the second is induced by the addition of KCl (30 mM), added where indicated. Exposure time for each image was 0.5 s. The medium was as in Figure 2, but EGTA was omitted and CaCl<sub>2</sub> (1 mM) was included.

(B) Mean rises of N33D1cpv  $\Delta R/R_0$  as measured by epifluorescence or by TIRF in GH3 cells transiently transfected with N33D1cpv. The mean values of  $\Delta R/R_0 \pm \text{SEM}$  of spontaneous oscillations were  $0.126 \pm 0.007$  and  $0.196 \pm 0.008$  for epifluorescence and TIRF, respectively. The corresponding values for KCl-dependent depolarization were  $0.239 \pm 0.012$  and  $0.367 \pm 0.019$ , respectively. The differences between the values measured by TIRF and epifluorescence, both for the KCl and for the spontaneous  $\Delta R/R_0$  peaks, are statistically different ( $p < 0.001$ ). In some experiments with GH3 cells, the basal value of the 540/480 nm emission ratio (measured either by TIRF or epifluorescence) was substantially larger than that measured in HeLa cells or other batches of GH3 cells. Similarly, the fluorescence emission ratio increases in those experiments, as induced by spontaneous action potentials or KCl, were proportionally larger. We have no explanation for this finding.

shown). Near plasma membrane events (at a depth of about 200 nm) can be more conveniently monitored by using total internal reflection fluorescence (TIRF). TIRF objective-based approach, with a theoretical penetration depth ranging from about 80 to 170 nm (Betzig et al., 2006), allows to perform, in parallel batches of cells with the same experimental set-up, both classical epifluorescence and TIRF measurements. Not only the mean peak Ca<sup>2+</sup> values at the OMM elicited by histamine in HeLa cells were indistinguishable whether measured by epifluorescence or TIRF, but also the mean peak Ca<sup>2+</sup> at the OMM, as elicited by activating the CCE (using the standard

protocol; Filippin et al., 2003), are very similar in near plasma membrane and more deeply located mitochondria ( $\Delta R/R_0$  of  $0.30 \pm 0.013$  and  $0.27 \pm 0.016$ , respectively;  $n = 20$ ). A pixel-by-pixel analysis was also carried out on TIRF and epifluorescence images during CCE. The percentage of hot pixels was low and indistinguishable in near plasma membrane and more deeply located organelles (data not shown).

To investigate whether there is an intrinsic problem in revealing with TIRF Ca<sup>2+</sup> influx-dependent [Ca<sup>2+</sup>] microdomains on the OMM, we performed epifluorescence and TIRF measurements using GH3 cells that express VOCCs, primarily of L type. In GH3 cells, Ca<sup>2+</sup> influx through VOCCs can be observed both in response to spontaneous action potentials and when induced by the addition of depolarizing concentrations of KCl. Figure 6A shows a typical response pattern of the N33D1cpv fluorescence signal in GH3 cells showing spontaneous or KCl-induced [Ca<sup>2+</sup>]<sub>c</sub> transients (as measured by epifluorescence or TIRF). The mean peak rises ( $\Delta R/R_0$ ) of both the spontaneous Ca<sup>2+</sup> oscillations and those induced by KCl were about 30% smaller when measured by epifluorescence, as compared to TIRF (Figure 6B). We estimated the mean [Ca<sup>2+</sup>] peak rises: for spontaneous oscillations, the [Ca<sup>2+</sup>] peaks were  $1.33 \pm 0.09 \mu\text{M}$  and  $0.72 \pm 0.06 \mu\text{M}$  for TIRF and epifluorescence, respectively. For KCl-induced depolarization, we obtained the following values:  $3.54 \pm 0.25 \mu\text{M}$  for TIRF and  $1.71 \pm 0.16 \mu\text{M}$  for epifluorescence.

We generated another OMM-located probe, N33D3cpv, with a higher Ca<sup>2+</sup> affinity. Again, the peak rises during CCE reported by this probe, as analyzed by TIRF, were indistinguishable from those revealed by epifluorescence (data not shown).

We further investigated this problem by using an indirect approach previously employed (Filippin et al., 2003; Montero et al., 2000). Cells transfected with aequorin targeted to the mitochondrial matrix were challenged twice with the same stimulus under conditions eliciting similar [Ca<sup>2+</sup>]<sub>c</sub> increases. If the rise in [Ca<sup>2+</sup>]<sub>m</sub> is homogeneous among mitochondria, the second stimulus should lead to less photon emission, but the calibrated [Ca<sup>2+</sup>]<sub>m</sub> signals should mirror those of the cytosol; on the contrary, if selective aequorin consumption occurs, the second challenge would be apparently monitored as a strongly reduced Ca<sup>2+</sup> peak. Figure 7A demonstrates that, in HeLa cells expressing cytosolic aequorin, after store depletion by CPA added in Ca<sup>2+</sup>-free medium, addition of extracellular CaCl<sub>2</sub> results in two [Ca<sup>2+</sup>]<sub>c</sub> increases that peaked at  $1.1 \pm 0.2 \mu\text{M}$  and  $1.6 \pm 0.2 \mu\text{M}$ , respectively.

A parallel experiment, carried out with cells expressing mitochondrial aequorin (Figure 7B), shows that the two successive peaks caused by CaCl<sub>2</sub> addition paralleled those of the cytoplasm, i.e.,  $20.3 \pm 2.1$  and  $30.1 \pm 1.3 \mu\text{M}$ , during the first and second CaCl<sub>2</sub> challenge, respectively. This is summarized by the histogram in Figure 7C. On the contrary, upon two successive histamine challenges, the cytosolic increases were very similar, whereas the second mitochondrial peak was ~50% smaller compared to the first (Filippin et al., 2003 and confirmed here).

The same rationale was then used in GH3 cells: aequorin-expressing cells were challenged successively with depolarizing KCl concentrations, and the amplitudes of the first and second cytosolic and mitochondrial [Ca<sup>2+</sup>] peaks were compared. The results were strikingly different from those obtained during

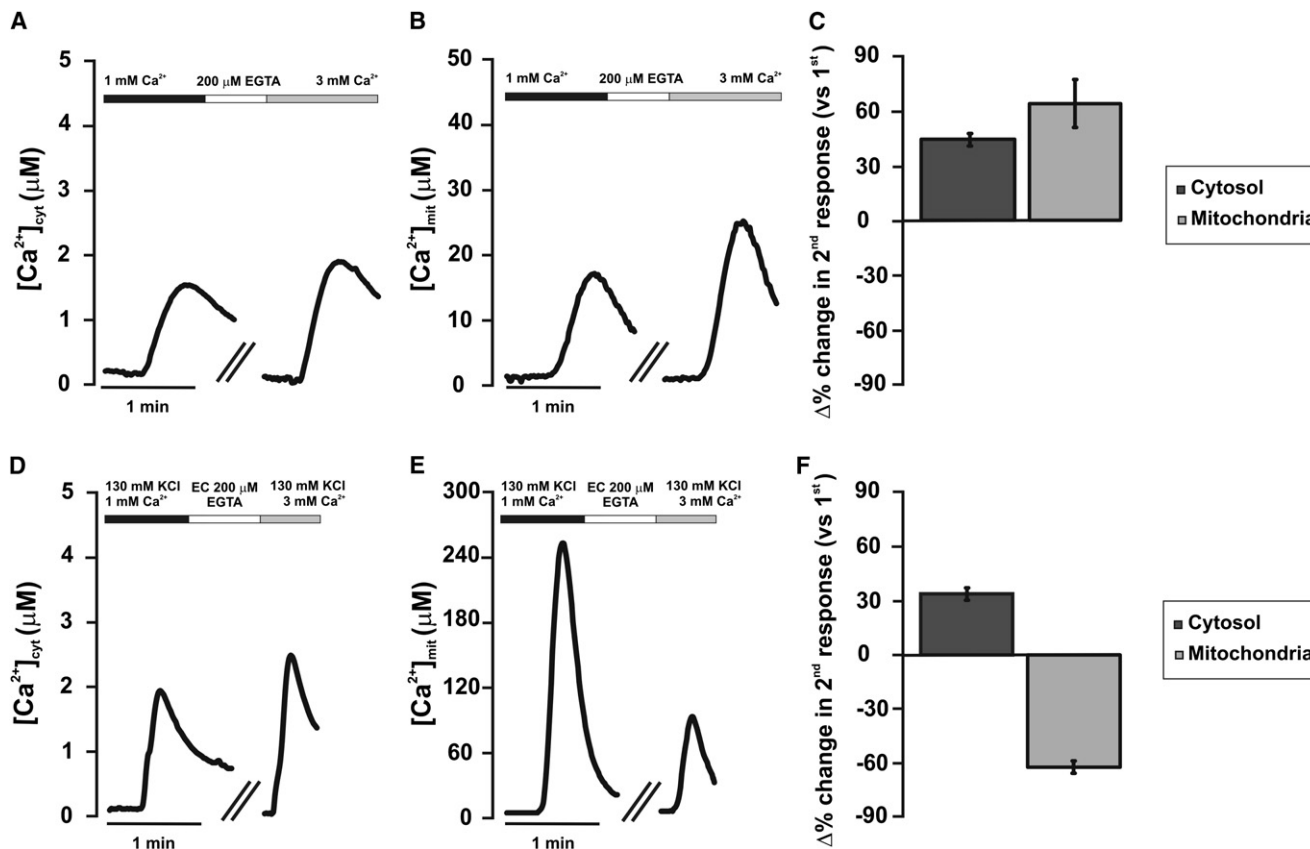


**Figure 7. Cytosolic and Mitochondrial Matrix [Ca<sup>2+</sup>] Increases, Measured with Targeted Aequorins, upon Activation of Ca<sup>2+</sup> Influx through CCE or VOCCs**

(A and B) HeLa cells expressing cytosolic (A) or mitochondrial (B) targeted aequorin were first treated with CPA (50  $\mu$ M) in a EGTA (200  $\mu$ M) containing medium, and CPA was maintained in the perfusing medium for the whole duration of the experiment. Where indicated, cells were perfused with medium containing 1 and 3 mM CaCl<sub>2</sub> in the first and second challenge, respectively. This protocol was chosen because a partial desensitization of CCE occurs within the time course of the experiment, and if 1 mM CaCl<sub>2</sub> was added also in the second challenge, the cytosolic peak was significantly smaller than the first (and so was the mitochondrial one).

(C) The percentage of the difference between the second and the first peak, normalized to the first one, was plotted for the cytosol (dark gray) and mitochondria (light gray). The error bars represent SEM.

(D and E) GH3 cells expressing cytosolic (D) or mitochondrial (E) targeted aequorin were perfused with a medium containing KCl (130 mM) in order to cause two successive depolarizations, as indicated by the bars. Again, due to partial desensitization in two successive KCl challenges, the CaCl<sub>2</sub> concentration of the second stimulation was higher than in the first, i.e., 3 and 1 mM, respectively.

(F) Same plot as (C) but refers to the Ca<sup>2+</sup> peaks caused in GH3 cells by two successive depolarizations. Cytosol (dark gray), mitochondria (light gray). The error bars represent SEM.

CCE: the first [Ca<sup>2+</sup>]<sub>c</sub> peak caused by KCl in GH3 cells was similar to that measured in HeLa cells (1.8  $\pm$  0.1  $\mu$ M; Figure 7D), but that of [Ca<sup>2+</sup>]<sub>m</sub> was  $\sim$ 10-fold higher (280.6  $\pm$  14.5  $\mu$ M; Figure 7E); the second KCl challenge elicited a [Ca<sup>2+</sup>]<sub>c</sub> peak of 2.4  $\pm$  0.06  $\mu$ M, whereas the [Ca<sup>2+</sup>]<sub>m</sub> peak was reduced to 40% of the first (Figure 7F). The reduction in amplitude of the second mitochondrial peak was clearly due to the selective consumption of aequorin in a pool of mitochondria and not to desensitization (or damage) of mitochondria during the first KCl challenge. Indeed, if the cells were transfected with mitochondrial aequorin and reconstituted with n-coelenterazine (that drastically reduces the consumption of aequorin for the same rise in [Ca<sup>2+</sup>]; Montero et al., 2000), the two successive KCl-induced peaks were very similar (data not shown).

## DISCUSSION

The importance of mitochondrial Ca<sup>2+</sup> accumulation in response to physiological or pathological increases in [Ca<sup>2+</sup>]<sub>c</sub> is now an established concept in biology (Bootman et al., 2001; Collins et al., 2001; Hajnóczky et al., 2006; Montero et al., 2000; Rizzuto et al., 1993; Rizzuto and Pozzan, 2006). Mitochondrial Ca<sup>2+</sup> accumulation, in fact, plays a key role in modulating the amplitude and kinetics of [Ca<sup>2+</sup>]<sub>c</sub> transients, the Ca<sup>2+</sup> activation/inactivation of Ca<sup>2+</sup> channels, and the intrinsic pathway of apoptosis. The general consensus is that living cells exhibit a highly efficient and rapid mitochondrial Ca<sup>2+</sup> uptake due to the strategic localization of mitochondria close to Ca<sup>2+</sup> hot spots. At present, however, this idea is supported only by a series of indirect

evidence. A number of key questions remain unanswered, for example: (1) What is [Ca<sup>2+</sup>] at the hot spots? (2) What percentage of the mitochondrial surface is exposed to the hot spots? (3) What is their duration?

Here, we have addressed these questions by generating a new probe (derived from the Dcpv family of GFP-based Ca<sup>2+</sup> sensors; Palmer et al., 2006), selectively targeted to the cytosolic side of the OMM.

The first finding was that the mean signal increases of OMM and cytosol upon stimulation with a Ca<sup>2+</sup>-mobilizing agonist such as histamine are very similar. We thus attempted a “pixel-by-pixel” analysis to compare cytosolic and OMM Ca<sup>2+</sup> responses. The first simplified approach suggests that the signal over the OMM is substantially heterogeneous during the upstroke of a histamine-induced Ca<sup>2+</sup> peak, whereas the frequency of Ca<sup>2+</sup> hot spots on the OMM, for the same Ca<sup>2+</sup> rise, is very low with a stimulus, like CPA, that causes passive Ca<sup>2+</sup> leak and thus no localized Ca<sup>2+</sup> increases. This analysis is, however, subject to major statistical uncertainties, and a more refined pixel-by-pixel correlation analysis was developed. To directly compare the Ca<sup>2+</sup> heterogeneity in different compartments, we used not only cells transfected in parallel with the cytosolic and OMM localized probes, but also in the very same cells, by cotransfecting N33D1cpv or D1cpv with another nuclear probe, H2BD1cpv. A vast body of data indicates that bulk nuclear and cytosolic [Ca<sup>2+</sup>] are in very rapid equilibrium (Rizzuto and Pozzan, 2006), though some debate still remains (Carafoli et al., 2001).

This approach revealed that: (1) Ca<sup>2+</sup> hot spots are found with a much higher probability close to mitochondria rather than in randomly chosen regions of the cytoplasm or nucleus; (2) the frequency of Ca<sup>2+</sup> hot spots varies among different mitochondria of the same cells; (3) the surface of mitochondria covered by Ca<sup>2+</sup> hot spots during the upstroke of a histamine challenge (i.e., within the first 4 s of the histamine peak) covers about 10% of the mitochondrial surface. This value is probably underestimated, given that out of focus mitochondria could not be considered in these epifluorescence images; and (4) the size of the hot spots, averaged over time and space is smaller than 1 μm<sup>2</sup>.

Given the different subcellular localization of N33D1cpv and D1cpv or H2BD1cpv, we also investigated whether the microenvironment of the two probes affects their Ca<sup>2+</sup> affinity. An *in situ* calibration was performed, using digitonin-permeabilized cells in a medium mimicking the ionic composition of the cytoplasm. Indeed, the microenvironment appears to partially modify the probe response to Ca<sup>2+</sup>; in particular, the dynamic range and the K<sub>d</sub> for Ca<sup>2+</sup> of N33D1cpv were slightly higher than those of H2BD1cpv. We concluded that: (1) the mean [Ca<sup>2+</sup>] experienced by the OMM upon histamine stimulation is substantially higher than that measured in the nucleoplasm or in the cytosol; and (2) the hot spots monitored on the OMM may reach values as high as 15–20 μM.

We also addressed the question of whether Ca<sup>2+</sup> rises close to the plasma membrane are higher than those occurring in the deep cytoplasm during Ca<sup>2+</sup> influx, taking advantage of the TIRF technique. In HeLa cells, the peak OMM Ca<sup>2+</sup> rises elicited by Ca<sup>2+</sup> influx due to CCE revealed minor differences between subplasma membrane mitochondria and organelles more deeply

located in the cells. It thus appears that mitochondria are excluded from the regions where the store-operated Ca<sup>2+</sup> channels (Orai1; Prakriya et al., 2006) are activated. This conclusion is consistent with the accepted model of Orai1 channel activation, i.e., the apposition of ER cisternae (via STIM1) to the plasma membrane (where Orai1 channels are clustered) (Liou et al., 2005; Luik et al., 2008; Roos et al., 2005; Zhang et al., 2005). According to this model, due to the close apposition between ER and plasma membrane, a physical barrier should preclude the access of mitochondria to the mouths of Orai1 channels. This conclusion is also consistent with recent morphological data (Korzeniowski et al., 2009). It is suggested that previous models in which mitochondria were thought to play a local Ca<sup>2+</sup> buffering role at the mouth of CCE channels must be revisited (Hoth et al., 1997; Parekh, 2003).

In order to confirm that the lack of Ca<sup>2+</sup> hot spots at the OMM of subplasma membrane mitochondria is due to exclusion of mitochondria from the ER-plasma membrane contact sites during CCE, we turned to another cellular model (GH3 cells). In this latter case, the [Ca<sup>2+</sup>] peak rises, elicited by opening of VOCCs, were twice as large in mitochondria close to the plasma membrane as in organelles more deeply located. It should be stressed that, due to the relatively slow time resolution of the apparatus, the [Ca<sup>2+</sup>] reported is the mean over 0.5 s, i.e., the OMM [Ca<sup>2+</sup>] at the peak of the Ca<sup>2+</sup> current is probably substantially underestimated. We have further addressed this problem by a double-stimulus challenge using cytosolic and mitochondrial (matrix) targeted aequorin. This approach, previously employed to support the existence of Ca<sup>2+</sup> microdomains around mitochondria (Montero et al., 2000), gave clear results: two successive similar [Ca<sup>2+</sup>]<sub>c</sub> increases resulted in a much reduced second [Ca<sup>2+</sup>]<sub>m</sub> peak when a double KCl (in GH3 cells) or histamine (in HeLa cells) challenge was applied; two successive similar cytosolic peaks elicited by CCE through store-operated Ca<sup>2+</sup> channels (in HeLa cells) resulted in two similar [Ca<sup>2+</sup>]<sub>m</sub> peaks. In addition, similar [Ca<sup>2+</sup>]<sub>c</sub> increases, when elicited by KCl depolarization or CCE, resulted in dramatically different [Ca<sup>2+</sup>]<sub>m</sub> peaks, about 10-fold higher in the former case. Both results are consistent with the generation of microdomains of high [Ca<sup>2+</sup>]<sub>c</sub> near the plasma membrane (and thus a major selective consumption of aequorin in the case of subplasma membrane mitochondria in GH3 cells challenged with KCl) and of a modest and rather homogeneous [Ca<sup>2+</sup>]<sub>c</sub> increase in subplasma membrane mitochondria in HeLa cells during CCE.

In conclusion, we here have directly demonstrated and quantitatively measured the formation of Ca<sup>2+</sup> microdomains on the mitochondrial surface close to plasma membrane or ER Ca<sup>2+</sup> channels. The [Ca<sup>2+</sup>] at the hot spots, as induced by Ca<sup>2+</sup> mobilization from stores, appears to be 5- to 10-fold higher than in the bulk cytosol, thus accounting for the efficient Ca<sup>2+</sup> uptake of a subpopulation of mitochondria during activation of Ca<sup>2+</sup> release in intact cells. We also demonstrate that these hot spots are of relatively long duration and that they are heterogeneously distributed in the mitochondrial network. As to mitochondria close to the plasma membrane, both the use of the TIRF technique and of aequorin targeted to the mitochondrial matrix indicate that activation of CCE does not result in a preferential increase of [Ca<sup>2+</sup>] of their OMM, suggesting the exclusion of

mitochondria from the regions very close to store-operated Ca<sup>2+</sup> channels. On the contrary, opening of VOCCs results in a larger [Ca<sup>2+</sup>] increase around subplasma membrane mitochondria than around organelles localized at distance from the cell surface.

## EXPERIMENTAL PROCEDURES

### Constructs

The sequence coding for the TOM20 protein was introduced before the His tag of D1cpv (kindly provided by R. Tsien, University of California, San Diego, CA) by digestion with HindIII and ligation onto the same site of pcDNA3 (Invitrogen). The N33 moiety was introduced by PCR amplification of the first 99 base pairs of TOM20. In order to introduce the H2B coding sequence, the cDNA coding for H2B-YFP (a kind gift of Dr. T. Kanda, Salk Institute, La Jolla, CA) was used as template. Oligonucleotides are listed in the [Supplemental Experimental Procedures](#). The resulting PCR products were digested with HindIII, ligated into the same sites of pcDNA3 (Invitrogen), and transformed into *Escherichia coli* (TOP10; Invitrogen).

### Cell Culture and Transfection

HeLa cells were grown in DMEM containing 10% FCS, 2 mM L-glutamine, 100 U/ml penicillin, and 100 µg/ml streptomycin in a humidified atmosphere containing 5% CO<sub>2</sub>, and GH3 cells were grown in the same medium supplemented with nonessential amino acids (Sigma). Cells were seeded onto glass coverslips of 24 mm diameter (for imaging experiments) or 13 mm diameter (for aequorin measurements). Transfection was performed at 70% confluence using the Ca<sup>2+</sup>-phosphate technique for HeLa cells, and GH3 cells were transfected as described in [Drago et al. \(2008\)](#) for imaging experiments or were electroporated with a microporator (Digital Bio) according to manufacturer's protocol for aequorin measurements. All experiments were performed 48 hr after transfection, except in the case of electroporated GH3 cells, for which the experiments were performed 24 hr after transfection.

### Fluorescence Imaging

Cells expressing the fluorescent probes were analyzed using an inverted fluorescence microscope (Zeiss Axioplan) with an immersion oil objective (63×, N.A. 1.40). Excitation light at 425 nm was produced by a monochromator (Polychrome II, TILL Photonics, Martinsried, Germany). The emitted light was collected through a beam splitter (OES s.r.l., Padua; emission filters HQ 480/40M [for CFP] and HQ 535/30M [for YFP]) and a dichroic mirror 515 DCXR. The beam splitter allows the collection of the two emitted wavelengths at the same time, thus preventing any artifact due to movement of the organelles. Filters and dichroic mirrors were purchased from Omega Optical and Chroma. Images were acquired using a cooled CCD camera (Imago, TILL Photonics) attached to a 12 bit frame grabber. Synchronization of the monochromator and CCD camera was performed through a control unit run by TILLvisION 4.0 (TILL Photonics). Pixel sizes of 0.2 × 0.2 or 0.4 × 0.4 µm were used in different experiments (depending on the fluorescence intensity of the image), and the results of the pixel-by-pixel analyses were very similar. Pixel-by-pixel analysis was carried out by an originally created software using MatLab. We noticed that, when N33D1cpv was strongly overexpressed, the morphology of mitochondria was substantially altered. In all experiments presented, only cells with a normal mitochondrial morphology were analyzed.

Cells were mounted into an open-topped chamber thermostated at 37°C and maintained in an extracellular medium containing (in mM): 135 NaCl, 5 KCl, 1 MgSO<sub>4</sub>, 0.4 KH<sub>2</sub>PO<sub>4</sub>, 10 glucose, and 20 HEPES (pH 7.4 at 37°C). Plasma membrane permeabilization was performed by treating cells 1 min with digitonin (100 µM) in an intracellular-like medium containing (in mM): 130 K-gluconate, 10 NaCl, 1 KH<sub>2</sub>PO<sub>4</sub>, 1 MgSO<sub>4</sub>, 20 HEPES (pH 7.0 at 37°C), and EGTA (100 µM). In the calibration experiments, after removing digitonin, the medium was changed with a Ca<sup>2+</sup> buffer containing (mM): 2 EGTA, 1 H-EDTA, 1 MgCl<sub>2</sub> and variable CaCl<sub>2</sub> concentrations up to a free [Ca<sup>2+</sup>] of 1.1 µM. Higher free [Ca<sup>2+</sup>] levels were obtained by adding CaCl<sub>2</sub> to a Ca<sup>2+</sup>-free buffer (without EGTA) and taking into account the contaminating [Ca<sup>2+</sup>] (measured by flame photometry).

For TIRF experiments, we used a commercial White-Light TIRF apparatus (Nikon Instruments, USA), mounted on Nikon TE2000-E stage (Nikon Instruments, USA). The total internal reflection at the glass coverslip-water interface was obtained by means of an objective-based approach (CFI Plan Apochromat TIRF 60×/1.45 oil), with a theoretical penetration depth ranging from about 80 nm to 170 nm. FRET recordings were obtained through a beam splitter (Dualview, Optical Insight, USA) with filters emission bands (535/30 nm for YFP and 470/30 nm for CFP) with a 505LD dichroic mirror. Images were collected by means of a back thinned CCD camera (MicroMax 512 BFT, Princeton Instruments, USA) with 500 ms exposure time.

### Immunocytochemistry

Cells were fixed in phosphate buffered saline (PBS) containing 4% paraformaldehyde for 20 min, permeabilized with precooled methanol for 10 min, and then treated with NH<sub>4</sub>Cl 50 mM for 10 min. After washing twice with PBS-BSA 3%, cells were incubated with the following antibodies diluted in PBS-BSA 1.5% for 1 hr at 37°C: 1:200 polyclonal anti-GFP (ABCAM), 1:50 monoclonal anti-cytochrome C (BD PharMingen); and 1:50 monoclonal anti-TOM20 (Santa Cruz Biotechnology). Samples were washed three times in PBS-BSA 0.5% and then treated with Alexa Fluor 568 goat anti-rabbit IgG or Alexa Fluor 555 goat anti-mouse IgG (Invitrogen) for 1 hr at room temperature.

In the case of digitonin treatment, after washing with PBS, cells were permeabilized with 100 µM digitonin in an intracellular-like medium containing 5% Dextran (Type 40) and EGTA 100 µM and were then fixed as previously described or incubated in the intracellular-like medium with the antibodies for 1 hr at 37°C. After this treatment, cells were fixed, and secondary antibody treatment followed. After treatment with secondary antibody, cells were washed three times in PBS-BSA 5% and three times in PBS, mounted with Mowiol (Sigma), and analyzed with a Video Confocal Microscope System (Biomedica Mangoni snc, Italy) using an immersion oil objective (60×/1.4 oil planapo VC; Nikon Instruments, USA). Image acquisition was performed with excitation wavelengths of 488 nm for N33D1cpv and 543 nm for Alexa Fluor 568 or Alexa Fluor 555.

### Aequorin Measurements

Transfected cells were incubated for 1–2 hr in extracellular medium supplemented with 5 µM coelenterazine and 1 mM CaCl<sub>2</sub> (HeLa cells) or 200 µM EGTA (GH3 cells). Aequorin measurement was performed as described in [Filippin et al. \(2003\)](#).

### Materials

CPA, histamine, and digitonin were purchased from SIGMA-Aldrich. All other materials were analytical or highest available grade.

### Statistical Analysis

All of the data are representative of at least ten different experiments unless otherwise indicated. Values are expressed as mean ± SD or mean ± SEM. Statistical significance was determined using the Student's t test. \*p < 0.05; \*\*p < 0.001.

## SUPPLEMENTAL INFORMATION

Supplemental Information includes Supplemental Experimental Procedures and five figures and can be found with this article online at [doi:10.1016/j.molcel.2010.04.003](https://doi.org/10.1016/j.molcel.2010.04.003).

## ACKNOWLEDGMENTS

This work was supported by grants from the Italian Ministry of University (2007BZ4RX3), the Veneto Region, The University of Padova (Strategic Project STPD085PM7), and the Italian Institute of Technology to T.P.; by University of Padova, grant number CPDR078721 to M.S.; and by Italian Ministry of University (FIRB 2004) to P.P.

Received: November 3, 2009

Revised: December 21, 2009

Accepted: February 3, 2010

Published: April 22, 2010

## REFERENCES

- Allbritton, N.L., Oancea, E., Kuhn, M.A., and Meyer, T. (1994). Source of nuclear calcium signals. *Proc. Natl. Acad. Sci. USA* *91*, 12458–12462.
- Babcock, D.F., Herrington, J., Goodwin, P.C., Park, Y.B., and Hille, B. (1997). Mitochondrial participation in the intracellular Ca<sup>2+</sup> network. *J. Cell Biol.* *136*, 833–844.
- Betzig, E., Patterson, G.H., Sougrat, R., Lindwasser, O.W., Olenych, S., Bonifacio, J.S., Davidson, M.W., Lippincott-Schwartz, J., and Hess, H.F. (2006). Imaging intracellular fluorescent proteins at nanometer resolution. *Science* *313*, 1642–1645.
- Bootman, M.D., Lipp, P., and Berridge, M.J. (2001). The organisation and functions of local Ca<sup>2+</sup> signals. *J. Cell Sci.* *114*, 2213–2222.
- Brandenburger, Y., Arrighi, J.F., Rossier, M.F., Maturana, A., Vallotton, M.B., and Capponi, A.M. (1999). Measurement of perimitochondrial Ca<sup>2+</sup> concentration in bovine adrenal glomerulosa cells with aequorin targeted to the outer mitochondrial membrane. *Biochem. J.* *341*, 745–753.
- Carafoli, E., Santella, L., Branca, D., and Brini, M. (2001). Generation, control, and processing of cellular calcium signals. *Crit. Rev. Biochem. Mol. Biol.* *36*, 107–260.
- Collins, T.J., Lipp, P., Berridge, M.J., and Bootman, M.D. (2001). Mitochondrial Ca<sup>2+</sup> uptake depends on the spatial and temporal profile of cytosolic Ca<sup>2+</sup> signals. *J. Biol. Chem.* *276*, 26411–26420.
- Drago, I., Giacomello, M., Pizzo, P., and Pozzan, T. (2008). Calcium dynamics in the peroxisomal lumen of living cells. *J. Biol. Chem.* *283*, 14384–14390.
- Filippin, L., Magalhães, P.J., Di Benedetto, G., Colella, M., and Pozzan, T. (2003). Stable interactions between mitochondria and endoplasmic reticulum allow rapid accumulation of calcium in a subpopulation of mitochondria. *J. Biol. Chem.* *278*, 39224–39234.
- Hajnóczky, G., Csordás, G., Das, S., Garcia-Perez, C., Saotome, M., Sinha Roy, S., and Yi, M. (2006). Mitochondrial calcium signalling and cell death: approaches for assessing the role of mitochondrial Ca<sup>2+</sup> uptake in apoptosis. *Cell Calcium* *40*, 553–560.
- Hoth, M., Fanger, C.M., and Lewis, R.S. (1997). Mitochondrial regulation of store-operated calcium signaling in T lymphocytes. *J. Biol. Chem.* *137*, 633–648.
- Kanaji, S., Iwahashi, J., Kida, Y., Sakaguchi, M., and Mihara, K. (2000). Characterization of the signal that directs Tom20 to the mitochondrial outer membrane. *J. Cell Biol.* *151*, 277–288.
- Korzeniowski, M.K., Szanda, G., Balla, T., and Spät, A. (2009). Store-operated Ca<sup>2+</sup> influx and subplasmalemmal mitochondria. *Cell Calcium* *46*, 49–55.
- Lawrie, A.M., Rizzuto, R., Pozzan, T., and Simpson, A.W.M. (1996). A role for calcium influx in the regulation of mitochondrial calcium in endothelial cells. *J. Biol. Chem.* *271*, 10753–10759.
- Liou, J., Kim, M.L., Heo, W.D., Jones, J.T., Myers, J.W., Ferrell, J.E., Jr., and Meyer, T. (2005). STIM is a Ca<sup>2+</sup> sensor essential for Ca<sup>2+</sup>-store-depletion-triggered Ca<sup>2+</sup> influx. *Curr. Biol.* *15*, 1235–1241.
- Luiik, R.M., Wang, B., Prakriya, M., Wu, M.M., and Lewis, R.S. (2008). Oligomerization of STIM1 couples ER calcium depletion to CRAC channel activation. *Nature* *454*, 538–542.
- Montero, M., Alonso, M.T., Carnicero, E., Cuchillo-Ibáñez, I., Albillos, A., García, A.G., García-Sancho, J., and Alvarez, J. (2000). Chromaffin-cell stimulation triggers fast millimolar mitochondrial Ca<sup>2+</sup> transients that modulate secretion. *Nat. Cell Biol.* *2*, 57–61.
- Orrenius, S., Zhivotovsky, B., and Nicotera, P. (2003). Regulation of cell death: the calcium-apoptosis link. *Nat. Rev. Mol. Cell Biol.* *4*, 552–565.
- Pacher, P., Thomas, A.P., and Hajnóczky, G. (2002). Ca<sup>2+</sup> marks: miniature calcium signals in single mitochondria driven by ryanodine receptors. *Proc. Natl. Acad. Sci. USA* *99*, 2380–2385.
- Palmer, A.E., Giacomello, M., Kortemme, T., Hires, S.A., Lev-Ram, V., Baker, D., and Tsien, R.Y. (2006). Ca<sup>2+</sup> indicators based on computationally redesigned calmodulin-peptide pairs. *Chem. Biol.* *13*, 521–530.
- Parekh, A.B. (2003). Store-operated Ca<sup>2+</sup> entry: dynamic interplay between endoplasmic reticulum, mitochondria and plasma membrane. *J. Physiol.* *547*, 333–348.
- Prakriya, M., Feske, S., Gwack, Y., Srikanth, S., Rao, A., and Hogan, P.G. (2006). Orai1 is an essential pore subunit of the CRAC channel. *Nature* *443*, 230–233.
- Rizzuto, R., and Pozzan, T. (2006). Microdomains of intracellular Ca<sup>2+</sup>: molecular determinants and functional consequences. *Physiol. Rev.* *86*, 369–408.
- Rizzuto, R., Brini, M., Murgia, M., and Pozzan, T. (1993). Microdomains with high Ca<sup>2+</sup> close to IP<sub>3</sub>-sensitive channels that are sensed by neighboring mitochondria. *Science* *262*, 744–747.
- Rizzuto, R., Pinton, P., Carrington, W., Fay, F.S., Fogarty, K.E., Lifshitz, L.M., Tuft, R.A., and Pozzan, T. (1998). Close contacts with the endoplasmic reticulum as determinants of mitochondrial Ca<sup>2+</sup> responses. *Science* *280*, 1763–1766.
- Rizzuto, R., Pinton, P., Ferrari, D., Chami, M., Szabadkai, G., Magalhães, P.J., Di Virgilio, F., and Pozzan, T. (2003). Calcium and apoptosis: facts and hypotheses. *Oncogene* *22*, 8619–8627.
- Rizzuto, R., Duchen, M.R., and Pozzan, T. (2004). Flirting in little space: the ER/mitochondria Ca<sup>2+</sup> liaison. *Sci. STKE* *2004*, re1.
- Roos, J., DiGregorio, P.J., Yeromin, A.V., Ohlsen, K., Lioudyno, M., Zhang, S., Safrina, O., Kozak, J.A., Wagner, S.L., Cahalan, M.D., et al. (2005). STIM1, an essential and conserved component of store-operated Ca<sup>2+</sup> channel function. *J. Cell Biol.* *169*, 435–445.
- Rudolf, R., Magalhaes, P.J., and Pozzan, T. (2006). Direct in vivo monitoring of sarcoplasmic reticulum Ca<sup>2+</sup> and cytosolic cAMP dynamics in mouse skeletal muscle. *J. Biol. Chem.* *173*, 187–193.
- Rutter, G.A. (2006). Moving Ca<sup>2+</sup> from the endoplasmic reticulum to mitochondria: is spatial intimacy enough? *Biochem. Soc. Trans.* *34*, 351–355.
- Sahlin, K., Jorfeldt, L., Henriksson, K.G., Lewis, S.F., and Haller, R.G. (1995). Tricarboxylic acid cycle intermediates during incremental exercise in healthy subjects and in patients with McArdle's disease. *Clin. Sci. (Lond.)* *88*, 687–693.
- Zhang, S.L., Yu, Y., Roos, J., Kozak, J.A., Deerinck, T.J., Ellisman, M.H., Stauderman, K.A., and Cahalan, M.D. (2005). STIM1 is a Ca<sup>2+</sup> sensor that activates CRAC channels and migrates from the Ca<sup>2+</sup> store to the plasma membrane. *Nature* *437*, 902–905.